T. Claquin · C. Roelandt · K.E. Kohfeld · S.P. Harrison
I. Tegen · I.C. Prentice · Y. Balkanski · G. Bergametti
M. Hansson · N. Mahowald · H. Rodhe · M. Schulz

Radiative forcing of climate by ice-age atmospheric dust

Abstract During glacial periods, dust deposition rates and inferred atmospheric concentrations were globally much higher than present. According to recent model results, the large enhancement of atmospheric dust content at the last glacial maximum (LGM) can be explained only if increases in the potential dust source areas are taken into account. Such increases are to be expected, due to effects of low precipitation and low atmospheric (CO_2) on plant growth. Here the modelled three-dimensional dust fields from Mahowald et al. and modelled seasonally varying surface-albedo fields derived in a parallel manner, are used to quantify the mean radiative forcing due to modern (non-anthropogenic) and LGM dust. The effect of mineralogical provenance on the radiative properties of the dust is taken into account, as is the range of optical properties associated with uncertainties about the mixing state of the dust particles. The high-latitude (poleward of 45°) mean change in forcing (LGM minus modern) is estimated to be small (-0.9 to $+0.2$ W m^{-2}), especially when compared to nearly -20 W m^{-2} due to reflection from the extended ice sheets. Although the net effect of dust over ice sheets is a positive forcing (warming), much of the simulated high-latitude dust was not over the ice sheets, but over unglaciated regions close to the expanded dust source region in central Asia. In the tropics the change in forcing is estimated to be overall negative, and of similarly large magnitude (-2.2 to -3.2 W m^{-2}) to the radiative cooling effect of low atmospheric (CO_2). Thus, the largest long-term climatic effect of the LGM dust is likely to have been a cooling of the tropics. Low tropical sea-surface temperatures, low atmospheric (CO_2) and high atmospheric dust loading may be mutually reinforcing due to multiple positive feedbacks, including the negative radiative forcing effect of dust.

T. Claquin · Y. Balkanski · M. Schulz
Laboratoire des Sciences du Climat et de l'Environnement,
L'Orme des Merisiers, Bâtiment 701,
F-91191 Gif-sur-Yvette cedex, France

C. Roelandt · K.E. Kohfeld · S.P. Harrison
I. Tegen · I.C. Prentice (✉)
Max-Planck Institute for Biogeochemistry,
PO Box 100164, D-07701 Jena, Germany
E-mail: colin.prentice@bgc-jena.mpg.de

C. Roelandt · S.P. Harrison
Dynamic Palaeoclimatology, Lund University,
Box 117, S-22300 Lund, Sweden

G. Bergametti
Laboratoire Interuniversitaire des Systèmes Atmosphériques;
Université Paris VII-Paris XII, URA CNRS 1404,
Centre multidisciplinaire de Créteil,
61, avenue du Général de Gaulle, F-94010 Créteil cedex, France

N. Mahowald · H. Rodhe
Department of Meteorology,
Stockholm University, S-10691 Stockholm, Sweden

M. Hansson
Department of Physical Geography and Quaternary Geology,
Stockholm University, S-10691 Stockholm, Sweden

N. Mahowald
Bren School of Environmental Science and Management,
University of California, Santa Barbara, CA 93106, USA

Present address: T. Claquin
EuroBios SA, Tour Ernst & Young,
F-92037 La Défense cedex, France

Present address: C. Roelandt
Department of Geography, Université catholique de Louvain,
Place Louis Pasteur 3, B-1348 Louvain-la-Neuve, Belgium

1 Introduction

Mineral aerosol (dust) in the atmosphere contributes to the radiative forcing of the present-day climate (Tegen and Fung 1994; Sokolik and Toon 1996). Deposition fluxes of dust at the last glacial maximum, LGM ($\approx$21,000 yr BP) were on average 2 to 20 times higher than modern values over most of the world (e.g. Thompson and Moseley-Thompson 1981; Rea 1994; DeAngelis et al. 1997; Petit et al. 1999), indicating a far higher long-term global atmospheric concentration of

dust than is observed at present. This study represents a first attempt to quantify the climatological mean radiative forcing due to dust at the LGM, and considers possible implications of this forcing for the mechanisms of glacial–interglacial climate change.

Modern and past accumulation rates of aeolian material in loess, marine sediments and ice cores provide a benchmark for numerical simulations of the dust cycle and its response to climate change (Mahowald et al. 1999). In so far as we can establish agreement between model results and observations, we can begin to attribute causes to the changes seen in the palaeorecord of dust. High levels of dust in the glacial atmosphere could in principle be explained by changes in atmospheric circulation (e.g. stronger winds), the strength of the hydrological cycle (decreased scavenging of dust particles, Yung et al. 1996), and potential source areas (increased unvegetated or sparsely vegetated regions with exposed dry soil). Model results by Andersen et al. (1998) and Mahowald et al. (1999) indicate that changes in source areas are an essential part of the explanation for the observed change in dust accumulation rates between LGM and present. Mahowald et al. (1999) in particular showed that the magnitude of the change in observed dust deposition fluxes can be reproduced when account is taken of the effects of low precipitation, in combination with physiological effects of low atmospheric (CO_2), on terrestrial plant productivity as simulated by the BIOME3 equilibrium biogeography–biogeochemistry model. Modelled changes in atmospheric circulation and the hydrological cycle were not sufficient to explain the observations, unless consequent changes in vegetation between LGM and present were allowed to influence the potential dust source regions. The simulations of Mahowald et al. (1999) succeeded in matching many specific geographic features of the LGM and modern dust distributions, including the large high-latitude amplification of the glacial–interglacial difference in aeolian fluxes, evident in records from the polar ice caps (e.g. DeAngelis et al. 1997; Petit et al. 1999). The three-dimensional dust fields as simulated by Mahowald et al. (1999) provided the starting point for the present study.

Radiative forcing by dust depends on aerosol optical properties (a function of particle size distribution and refractive index) and the albedo of the underlying surface, including liquid cloud cover (Quijano et al. 2000). The top-of-the-atmosphere (TOA) forcing due to dust is generally negative (implying potential cooling) because of short wave backscattering, but it can reach positive values (implying potential warming) when the underlying surface albedo is high, or when the absorption of short- and longwave radiation by the aerosol particles is substantial. Because of the likely sensitivity of radiative forcing by dust to changes in land surface conditions between LGM and modern conditions, we simulate seasonally varying fields of modern and LGM land-surface albedo that are consistent with the vegetation patterns obtained by Mahowald et al. (1999). We use

these simulated fields in the radiative calculations. The largest uncertainty concerning aerosol optical properties however stems from the scarcity of atmospheric measurements documenting the relationship between mineralogical composition of particles and their radiative properties (Tegen and Lacis 1996; Claquin et al. 1998; Sokolok and Toon 1999). Our calculation of radiative forcing takes into account the influence of mineralogical provenance on dust optical properties (Claquin et al. 1999). We also consider the different optical properties possible due to different mixing states of the minerals, particularly the disposition of haematite. The presence of haematite can significantly increase the optical absorption of dust particles by forming an internal mixture, in which this dark-coloured mineral tends to form a coating over the particle surface. We therefore make bounding calculations, using the alternatives of external mixing (i.e. all minerals separate), and internal mixing of haematite.

2 Methods

2.1 Climate, vegetation and potential dust source regions

The BIOME3 model (Haxeltine and Prentice 1996) was used to simulate dust source regions. BIOME3 is an equilibrium biogeography model that predicts the large-scale distribution of major terrestrial ecosystem types (biomes) as a function of climate, soil properties and atmospheric (CO_2). In BIOME3, an initial "sieve" selects the plant functional types (PFTs) that can occur in a given environment, based on specific tolerances (such as the low temperature limits for different frost resistance mechanisms). Then, for each grid cell, the model computes multiple values of annual net primary production (NPP). These values correspond to different assumptions about the dominant PFT and its leaf area index (LAI). The NPP calculations are based on a mean seasonal cycle of photosynthesis and plant respiration. Leaf-level photosynthetic capacity is determined according to optimal nitrogen allocation theory. Photosynthesis is calculated using a simultaneous solution of the biochemical (Farquhar) and diffusion equations. Stomatal conductance satisfies both the Monteith (1995) parametrization of the relation between evapotranspiration and bulk surface conductance, and a representation of evapotranspiration as the lesser of the atmospheric water "demand" (Monteith 1995) and the soil "supply", a linear function of volumetric soil moisture and a PFT-dependent maximum transpiration rate. PFTs differ in several further parameters including phenological rules, photosynthetic pathway, and parameters affecting the inhibition of photosynthesis at high and low temperatures. The PFT selected as dominant, and the associated values of NPP and LAI, correspond to the combination of PFT and LAI that produces the largest NPP and is therefore considered the most competitive, with the proviso that tree PFTs are assumed to outcompete herbaceous PFTs wherever soil moisture and NPP are sufficient for forest growth. A set of empirical rules finally translates information on the dominant and subdominant PFTs and their relative NPP values into a biome assignment.

The modern vegetation distribution was obtained with BIOME3 using an observed modern climatology. A scenario for the LGM climate was obtained by an anomaly method, as described in Mahowald et al. (1999). That is, for each monthly climate variable, differences between mean values simulated by an atmospheric model for LGM and modern conditions were used to perturb the observed modern climatology. This procedure, widely used in climate impact studies, is designed to eliminate the direct influence of biases in the atmospheric model's simulation of modern climate. It

also allows a rough downscaling by simple interpolation from climate anomaly values at the grid of the atmospheric model to the finer (0.5°) grid of BIOME3. This downscaling is artificial, in the sense that it cannot produce reliable fine-scale boundaries, but it is nevertheless useful in the present context because the complexity of topography, the relatively small extent of dust sources, and the nonlinear (threshold) relation between dust deflation and vegetation density, could combine to give unstable estimates of source areas if all calculations were made on the atmospheric model grid. The estimated source areas, computed as a Boolean field at the 0.5° grid, are subsequently upscaled again as fractional areas at a coarse grid scale for modelling atmospheric transport.

In the modern case, the CLIMATE 2.0 (W. Cramer personal communication 1998) data set was used to provide the driving data for BIOME3. CLIMATE 2.0 is a 0.5° gridded climatology of monthly mean temperature, precipitation and fractional sunshine hours, which has been extensively used for terrestrial ecosystem modelling and model intercomparisons. CLIMATE 2.0 is an update of the published Leemans and Cramer (1991) climatology, but it is based on a much larger weather-station data set. Also, unlike Leemans and Cramer (1991), CLIMATE 2.0 uses a three-dimensional interpolation technique (piecewise thin-plate smoothing splines) to adjust each monthly climate variable for elevation effects. The resulting vegetation map produced with BIOME3 substantially agrees with present-day patterns of potential natural vegetation (Haxeltine and Prentice 1996).

The LGM climate scenario was derived from the ECHAM3 atmospheric general circulation model (AGCM under the Palaeoclimate Modelling Intercomparison Project (PMIP) protocol (Pinot et al. 1999). The LGM boundary conditions specified by the PMIP protocol are as follows: 21,000 yr BP insolation (Berger and Loutre 1991), CLIMAP sea-surface temperatures (CLIMAP Project Members 1981), ICE-4G ice-sheet extent, height and sea-level equivalent (Peltier 1994), and atmospheric (CO_2) set to 200 ppm. The atmospheric (CO_2) prescribed to BIOME3 was also lowered to 200 ppm in order to account for the effects of low (CO_2) on productivity and canopy conductance, which limit the sustainable LAI in any given climate (Cowling 1999). The resulting LGM vegetation map shows generally satisfactory agreement with LGM vegetation patterns reconstructed from pollen and plant macrofossil data as part of the International Geosphere–Biosphere Programme project BIOME 6000 (Kohfeld and Harrison 2000; Prentice et al. 2000).

Potential dust source regions are regions in which vegetation is sparse due to inadequate moisture supply, and/or inadequate warmth. Sparse vegetation is indicated in BIOME3 by low values of LAI. When moisture supply is limiting, LAI is low because the advantage of higher LAI in increasing light capture is outweighed by the adverse effect of increased water use. When temperature is limiting, LAI is low because the potential growth is inadequate to sustain a higher leaf biomass. We defined the dust source areas as being all 0.5° grid cells where computed annual-maximum leaf area index (LAI) < 0.35 (for tropical or temperate biomes), or < 0.20 (for cold biomes). The LAI threshold for cold biomes is lower so as to compensate for a known tendency of BIOME3 to underestimate NPP at low temperatures. Within these potential dust source regions, monthly maximum soil moisture criteria for dust deflation on sand, silt and clay soils were defined in terms of relative soil moisture content of the uppermost soil layer (W/W_{max}) as 0.2, 0.25 and 0.5 respectively, following Tegen and Fung (1994). These choices of threshold values for LAI and W/W_{max} give an acceptable simulation of the large-scale patterns of present-day natural sources of dust (Mahowald et al. 1999).

2.2 Dust deflation and transport

The offline atmospheric tracer transport model TM3 (Heimann 1995; Schulz et al. 1998) was used to simulate global dust transport. TM3 has 3.75° × 5.0° horizontal resolution and 19 vertical levels. Tracer advection is computed using the slopes scheme (Russell and Lerner 1981) and mixing is computed for dry and moist convection. Wind speeds (u) for modern and LGM climates were read in from

ECHAM3 at 12 h intervals. Dust deflation was taken as proportional to u^3 for $u > 5$ m s^{-1}, and proportional to the fractional area of each grid cell occupied by active dust sources. Snow cover was assumed to suppress deflation. Dust was removed from the atmosphere by both dry and wet deposition (Mahowald et al. 1999). Total global dust emission by soils was adjusted to 3 Pg yr^{-1} (see Tegen and Fung 1994 for a discussion of the 0.2 to 5 Pg yr^{-1} range found in the literature).

Transport modelling for dust has to take account of the fact that dust particles vary in size over several orders of magnitude. This aspect was dealt with in a computationally efficient manner using the spectral scheme of Schulz et al. (1998), assuming a lognormal particle-radius distribution with a standard deviation of 2.0. The mean of the distribution is allowed to vary during transport. This scheme has been shown to give results as accurate as those from "bin" schemes (in which the aerosol is treated as being composed of a number of fixed size classes) while producing a severalfold gain in computational efficiency (Schulz et al. 1998), provided that attention focuses on grains of radius < 10 μm, which are overwhelmingly dominant in determining the radiative forcing due to airborne dust.

2.3 Surface albedo

Monthly sea-surface albedo values were obtained directly from ECHAM3. To account for the effect of simulated vegetation changes on land-surface albedo, we modelled land-surface albedo based on the modern and LGM climatologies and on biome distributions from BIOME3. Generic values of vegetation (A_v) and ground (A_g) albedos and vegetation roughness length (z_{ov}) were prescribed for each biome. Snow albedo (A_s) was assumed to decline exponentially with time, due to melting, whenever daily surface temperatures exceed -2 °C (Haxeltine and Prentice 1996). Under freezing conditions the albedo of snow was assumed to decline linearly due to ageing, following the parametrization of Douville et al. (1995a, b). Fractional areas of vegetation and bare ground were estimated from modelled LAI, using Beer's law. Snow-covered fraction of vegetation was estimated on a daily time step as $H_s/(H_s + 5z_{ov})$, where H_s is snow depth (m). Snow-covered fraction of bare ground was estimated as $W_s/(W_s + 50)$ where W_s is snow water equivalent (mm) (Douville et al. 1995a, b). The grid cell albedo was obtained as the area-weighted average of A_v, A_g and A_s. This approach to modelling snow cover and surface albedo has been tested (Roelandt, 2002 in press) against ERBE observations for albedo (Barkstorm et al. 1990) and with the ETAC data set for snow (Foster and Davy 1988). Zonal mean albedo values simulated in this way underestimate the ERBE-derived annual average albedo slightly (by 1 to 4%), while showing good agreement with the observed seasonal cycle. Simulated snow cover is slightly too persistent on the Northern Hemisphere land masses during spring (April to June), and otherwise shows good large-scale agreement with the ETAC data.

2.4 Optical properties and radiative forcing due to dust

For each grid cell of the TM3 model, the average dust mineralogy was calculated (Claquin 1999) based on a previous modelling study (Claquin et al. 1999) of the mineralogical composition of desert soils. Six minerals with distinct optical properties, i.e. quartz, calcite, haematite, illite, kaolinite and smectite, were considered. Dust mineralogy was assumed to be largely determined by soil parent material, and to have remained constant between the LGM and present.

Refractive indices for the minerals are presented in Claquin (1999). The single scattering albedo (ω) of dust is largely determined by the content of haematite and goethite, both of which absorb strongly in the visible waveband. When minerals are considered as an external mixture the single scattering albedo of dust is estimate to be on average 0.99 (0.98 to 1.00) over most regions. When the minerals are considered as an internal mixture,

with 3% haematite uniformly coating the grain of dust, the averaged value for ω decreases to 0.94 due to the larger surface area of haematite. Thus, the single scattering albedo of dust is estimated to lie within the range 0.94 to 0.99. These values are higher than those used in previous work (0.85–0.95), based on the work of Patterson (1981) and Volz (1973). The values we now compute for ω are consistent with a recent observational study on Saharan dust (Kaufmann et al. 2001). They measured reflectance by Saharan dust from Landsat 5 and extinction at the ground by sunphotometer measurements from the AERONET network. They obtained $\omega = 0.97$ at 640 nm, compared to older estimates ≈ 0.87 at the same wavelength.

Radiative forcing at the top-of-the-atmosphere was computed taking into account both solar (0.3 to 4 µm) and infrared radiation (> 4 µm) (Fouquart and Bonnel 1980; Morcrette and Fouquart 1985; Morcrette et al. 1986). The radiative code is based on a two-stream approximation and covers the infra-red and visible spectra in eight bands (Claquin et al. 1998). The infrared model is composed of six spectral bands. For each of these bands the fluxes are tabulated using the highly resolved code described in Morcrette and Fouquart (1985). Cloud, humidity and temperature fields for the radiative calculation were read in directly from ECHAM3 for both LGM and present.

2.5 Dust accumulation rates: the DIRTMAP data set

The DIRTMAP data set (Mahowald et al. 1999; Kohfeld and Harrison 2000, 2001) as used in this work contains 363 modern or LGM observations of the mass accumulation rate (MAR) of aeolian mineral material in marine and ice cores, or on land in the form of loess. The MAR in marine cores was defined as the product of bulk density, sedimentation rate and terrigenous fraction. Non-carbonate accumulation rates from Catubig et al. (1998) were included. In certain regions these may be inflated by the presence of marine biogenic SiO_2 (opal); however, exclusion of these data within the region over which opal is preserved at depth was found not to materially affect the patterns of MAR.

3 Results

3.1 Dust loading: simulated optical depth and observed accumulation rates

The three-dimensional dust fields of Mahowald et al. (1999) were used to generate estimates of total column optical depth at 550 nm (τ_{550}) (Figs. 1, 2a–c). Modelled τ_{550} in the modern climate shows a large peak in the northern subtropics, shifting by about 10° of latitude with the seasonal movement of the subtropical anticyclone and intertropical convergence zone (Fig. 1c). This behaviour is in good agreement with satellite measurements (Husar et al. 1997; Hermann et al. 1997). Figure 1c also indicates 14-year average locations of seasonal maxima in the absorbing aerosol index derived from the Total Ozone Mapping Spectrometer satellite instrument (TOMS AI) (Hermann et al. 1997). The magnitude of the TOMS AI depends on optical depth, aerosol height and optical properties, and clouds; however, even with partial cloud cover, the presence of absorbing aerosol can be detected. The TOMS AI signal in the northern subtropies and tropics is dominated by dust.

Modelled annual mean τ_{550} for the LGM was greater than modern at all latitudes (Figs. 1b, 2a–c). The
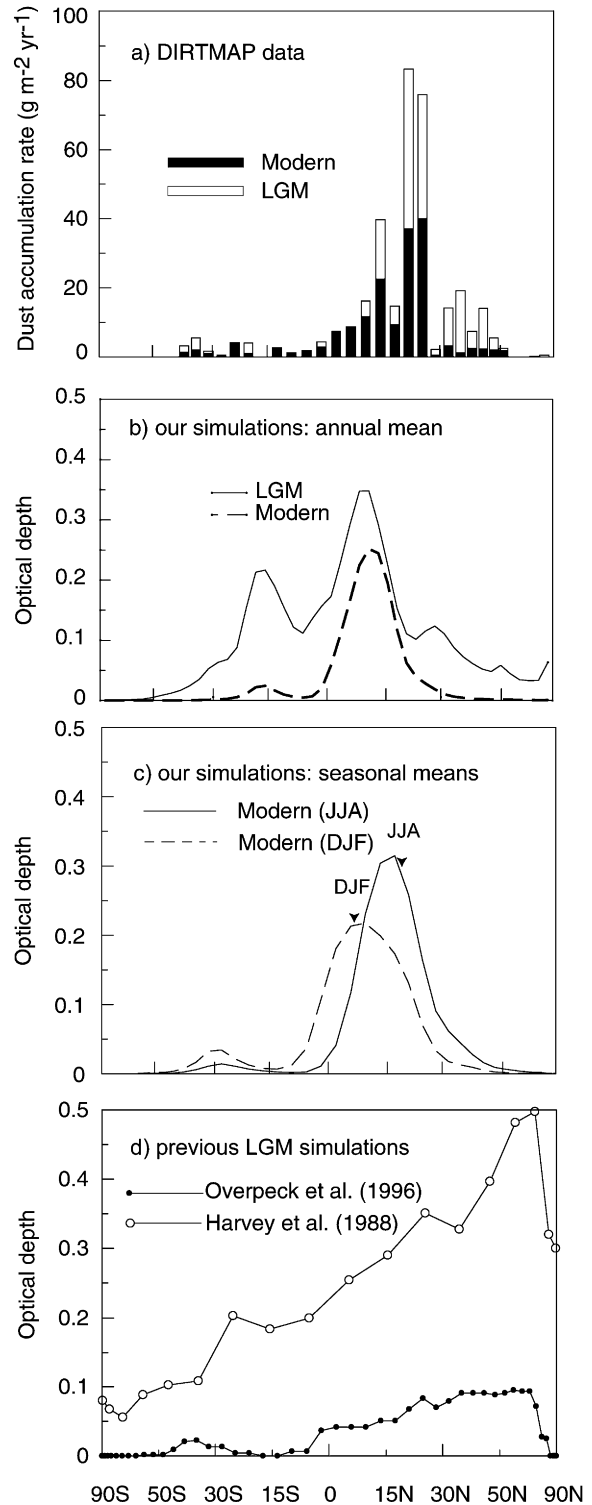
Fig. 1 Zonal averages: **a** observed modern and LGM dust accumulation in loess, marine sediments and ice, from DIRTMAP. **b** Modelled annual-mean optical depths due to natural dust sources. **c** Modelled seasonal mean optical depths for the modern climate. The arrows indicate the average 1979–1992 location of seasonal maxima in the absorbing aerosol index derived from the Total Ozone Mapping Spectrometer satellite instrument (Herman et al. 1997). **d** Optical depths calculated from the seasonally invariant dust fields used in earlier model sensitivity tests for the possible impact of LGM dust
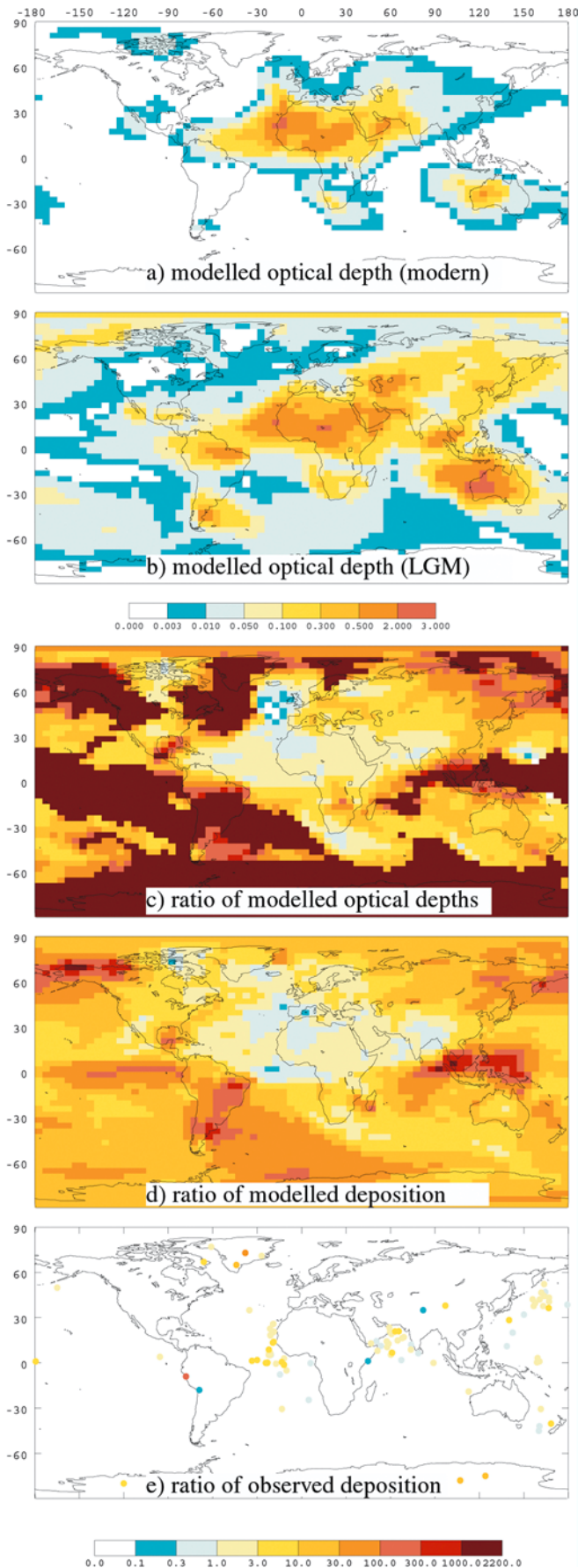
Fig. 2 Modelled annual mean optical depths due to natural dust sources for **a** modern climate, **b** LGM climate, **c** ratio LGM/modern. The modelled ratios of dust deposition **d** can be compared with **e** observed LGM/modern ratios of dust deposition rates, from DIRTMAP

latitude of the simulated dust maximum changed little, but the zone of simulated maximum dust loading at the LGM was extended by about 7 to 8° towards the south. This equatorward extension of the dust plume is confirmed by offshore dust records (e.g. Sarnthein et al. 1981; Ruddiman 1997). An additional simulated dust peak appears in the southern mid-latitudes due to the enlargement of the Patagonian and Australian deserts (both features confirmed by pollen and geomorphic evidence: Markgraf 1993; McTainsh and Lynch 1996) and stronger simulated winds.

These simulated zonal patterns and their changes between LGM and modern climates are consistent with the zonal patterns of observed recent and LGM dust accumulation rates (Figs. 1a, 2d,e). Observations support the geographic features seen in the simulated dust fields (Fig. 2d), including increased offshore transport from the Sahara (Kolla et al. 1979; Ruddiman 1997) and Australia (Hesse 1994) during the LGM, and an enhancement in the amount of dust transported from central Asia to high northern latitudes (Rea and Leinen 1988; Biscaye et al. 1997; Fig. 2e). General consistency between the simulated increase in dust source areas and the palaeovegetation evidence for widespread LGM aridity in the tropical continents (Farrera et al. 1999) suggests that the simulation of generally increased dust loadings in the tropics is reasonable. Dust accumulation rate data (Fig. 2e) support this finding for the Arabian Sea and the tropical Atlantic, where data are abundant. We are however lacking data from some tropical regions where the model shows large increases in dust loading, notably southeast Asia, southern Brazil and the equatorial Pacific.

Dust accumulation rate data from the Southern Hemisphere tropics are sparse. However, based on the limited data available, the overall magnitude of the Southern Hemisphere dust peak at the LGM appears to be overestimated by the simulation. In particular, the Australian dust source is overestimated. Dust in East Antarctic ice cores has been attributed to Patagonian sources (Basile et al. 1997), whereas in our simulation as much as half of the dust deposited at these sites originates from Australia. Although the provenance of dust in West Antarctica is not yet determined, quartz accumulation rates northwest of Australia (Kolla and Biscaye 1977) and dust accumulation rates in the Tasman Sea (Hesse 1994) suggest that LGM deposition rates exceeded present rates by a factor of 3 to 8. The model results indicate increases by a factor of 20 to 200. Comparison with palaeovegetation data for the LGM (Pickett et al. submitted)

confirms that Australian aridity was exaggerated in these simulations, due to underestimation of precipitation by ECHAM3 and/or underestimation of the water holding capacity of some soil types in BIOME3.

Figure 1d illustrates dust optical depth fields used in earlier sensitivity studies on the potential effects of LGM dust (Harvey 1988; Overpeck et al. 1996). Comparison with Fig. 1a immediately reveals that both studies greatly over-represented the amount of dust in the high northern latitudes relative to the tropics and subtropics (see also Table 1). According to our simulations (Figs. 1, 2), although the dust accumulation rate over (for example) Greenland was greatly amplified at LGM (consistent with ice-core records), the *absolute* atmospheric dust loading was still very small, and was slight compared with regions nearer to the major sources of dust.

3.2 Factors modifying the radiative effects of dust: particle size distribution and surface albedo

Simulated particle size distribution in regions distant from the major dust sources did not change substantially between LGM and modern climates (mass median diameter $\approx 2\,\mu$ min both regimes). Greenland ice-core data confirm that modal particle diameter changed by less than 0.3 μm between LGM and modern regimes (Steffensen 1997). Marine sediment data lead to the same conclusion, showing no significant correlation between flux density and particle size of aeolian material on glacial–interglacial time scales (Rea 1994).

The simulated surface albedo field (not shown) changed substantially, however, due to the presence of large ice sheets, extended sea ice, increased duration of snow cover, and exposure of continental shelf regions at the LGM. Vegetation changes, including large reductions of forest area and increases in tundra, steppe and desert biomes (consistent with observations as summarized e.g. by Prentice et al. 2000), further modified the surface albedo. As a result of these changes, simulated continental-surface albedo values were on average appreciably higher than modern values at high latitudes, and slightly higher even in the tropics.

3.3 Simulated radiative forcing by dust

We performed three main experiments as follows:

1. In experiment 1, all minerals were assumed to be externally mixed (i.e. quartz and haematite present as separate grains, transported independently), yielding the lowest radiation absorption, and therefore the most negative TOA forcing (largest potential cooling). This assumption likely represents a lower limit of absorption.
2. Experiment 2 assumed internal mixing of haematite (i.e. grains coated with haematite), which yields the highest radiation absorption, and therefore the strongest tendency toward positive TOA forcing (poential warming) over bright surfaces. This assumption likely represents an upper limit of absorption.

These two experiments bracket the most important uncertainty concerning the optical properties of mineral aerosol.

3. Experiment 3 assumed external mixing, like experiment 1, but optical depths over the Australian sector (60–180°E, 0–90°S) were reduced by a factor of 4.5. This rescaling renders the mean simulated LGM dust MAR over the seas surrounding Australia approximately equal to the mean observed rate based on marine sediment cores in the same region. This change is expected to lead to a somewhat more realistic estimate of the radiative forcing due to LGM dust in the affected region.

Table 1 Modelled annual and zonal mean optical depths and radiative forcing – summary of results. (Δ = LGM minus modern)

Latitude band	Optical depth (τ_{550})			TOA forcing (W m^{-2})							
	This study		Overpeck et al. (1996)	Effect of dust						Other effects Hewitt and Mitchell (1997)	
	Modern	LGM	LGM	Modern (Exp 1)	LGM (Exp 1)	Δ (Exp 1) External mixing	Δ (Exp 2): Internally mixed haematite	Δ (Exp 3): Australia dust reduced	Δ (Exp 4): Surface albedo unchanged	Δ low [CO$_2$]	Δ Insolation and albedo
45–90°N	0.00	0.07	0.08	−0.1	−1.0	−0.9	−0.3	−0.9	−1.2	−1.5	−18.8
15–45°N	0.13	0.19	0.07	−2.7	−4.2	−1.5	−0.8	−1.4	−1.9	−1.7	−3.7
0–15°N	0.14	0.26	0.04	−4.5	−7.7	−3.2	−2.3	−3.2	−3.8	−1.8	−2.0
0–15°S	0.01	0.13	0.00	−0.2	−3.5	−3.3	−2.1	−2.0	−3.7	−1.8	−2.0
15–45°S	0.01	0.15	0.01	−0.2	−2.9	−2.7	−1.1	−1.0	−3.1	−1.8	−2.0
45–90°S	0.00	0.02	0.00	0.0	−0.3	−0.3	+0.2	−0.3	−0.4	−1.5	−4.5
Global	0.05	0.14	0.03	−1.2	−3.2	−2.0	−1.0	−1.4	−2.3	−1.7	−5.2

In addition, we performed a sensitivity test:

4. Experiment 4 assumed external mixing, like experiment 1, but used modern surface albedo to compute the LGM radiative forcing. This experiment was designed to quantify the effect of surface albedo changes on the radiative forcing due to dust.

At high latitudes, the simulated annual average change in radiative forcing, LGM minus modern (Table 1; Fig. 3) in experiment 1 was negative: -0.9 W m^{-2} poleward of 45°N and -0.3 W m^{-2} poleward of 45°S. Experiment 2 also showed negative forcing in northern high latitudes, albeit smaller (-0.3 W m^{-2} poleward of 45°N), and showed a small positive forcing in southern high latitudes ($+0.2$ W m^{-2} poleward of 45°S). These results suggest that the mean LGM dust loading in the high latitudes produced a relatively minor, and probably overall negative, radiative effect. Recent work suggesting a somewhat reduced extent of continental (Moller et al. 1999) and sea (Weinelt et al. 1996; Crosta et al. 1998a, b) ice at the LGM implies a smaller "bright" area and therefore points in the direction of still more negative forcing by dust in the zonal average at high latitudes. The simulated forcing over the ice sheets themselves is nevertheless consistently positive, as in the model experiment of Overpeck et al. (1996).
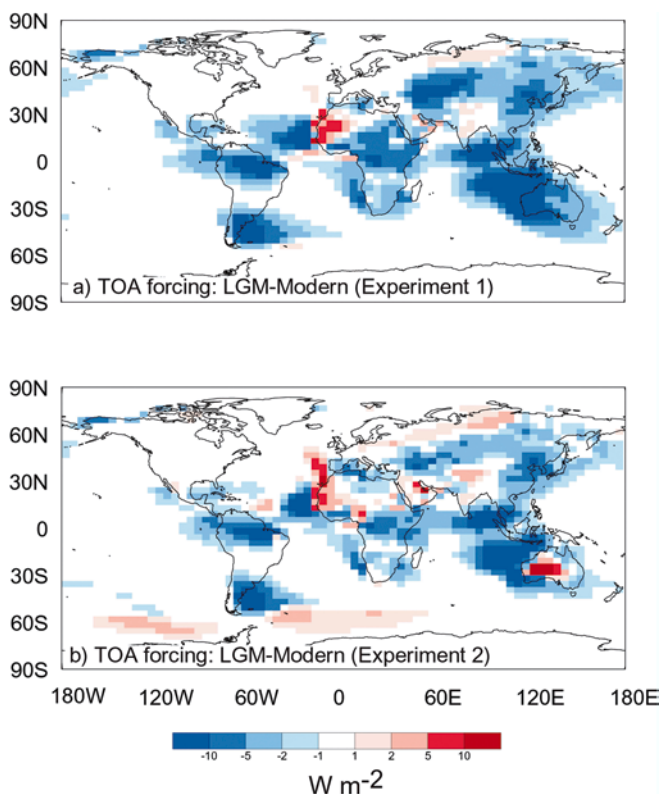
Over the tropics, the simulated radiative forcing of the LGM climate is of much larger magnitude than the forcing in high latitudes. The LGM radiative forcing is estimated to be -2.2 to -3.2 W m^{-2} more negative than present (based on experiments 1 and 2, to bracket the mixing assumptions) when averaged between 15°N and 15°S (Table 1). Both experiments show coherent structure with some areas showing very large negative anomalies (locally <-20 W m^{-2} over some ocean regions), and other areas with (generally smaller) positive anomalies ($>+5$ W m^{-2} over some desert regions) (Fig. 3). The simulated spatial patterns are similar in the two experiments, but experiment 2 with internal mixing of haematite shows generally weaker negative forcing anomalies, and a larger area with positive anomalies.

Experiment 3 with reduced dust in the Australian sector shows about 40% smaller negative forcing south of the equator. The tropical average effect of dust in the externally mixed case is reduced from -3.2 to -2.6 W m^{-2}.

Experiment 4 quantifies the importance of surface albedo changes on the radiative forcing due to dust. These changes reduce the magnitude of negative forcing at all latitudes, but the consequences are shown to be minor compared to the first-order radiative effects of dust.

4 Discussion

4.1 Interannual variability and the role of dust over ice sheets

Comparison of estimated radiative forcing anomalies due to features of the LGM environment apart from dust (Table 1; Hewitt and Mitchell 1997) shows that in high latitudes, the zonal average radiative forcing due to dust was one to two orders of magnitude smaller than the large negative (albedo) forcing due to more extensive snow and sea-ice cover and the presence of large continental ice sheets. This result appears superficially to conflict with that of Overpeck et al. (1996). They applied a uniform, enhanced dust cloud selectively over the LGM ice sheets, and they showed the resulting potential for a destabilizing warming due to dust. However, our results agree with Overpeck et al. (1996) to the extent that both studies show the sign of the radiative forcing due to dust over the ice sheets to be positive.

Further, we set out to simulate mean conditions during a period of two millenia around the LGM. Overpeck et al. (1996) in contrast set out to test the maximum effect of dust "spikes" as observed in the Greenland ice-core record. Some of these spikes show deposition enhanced by a further order of magnitude, for a period of years to decades, compared with the LGM baseline. The causes of this large interannual/interdecadal variability in Greenland dust have not been firmly established. For example, although our results show relatively little dust over the Laurentide and Scandinavian ice sheets and greater dust loadings over

Fig. 3 Modelled annual mean difference in radiative forcing at the top of the atmosphere (TOA), LGM minus modern, based on the optical depth fields in Fig.2. **a** experiment 1, assuming external mixing of minerals in the aerosol. **b** Experiment 2, assuming internal mixing of haematite

unglaciated Siberia due to the proximity of major dust sources in Central Asia (Fig. 2), we do not know whether any mechanism exists that could transport sufficient dust over the Laurentide ice sheet over a period of years to decades to meet the requirements of the Overpeck et al. (1996) hypothesis. Future modelling work could usefully attempt to determine the possible causes and characteristics of the dust spikes observed in high latitudes during glacial times.

4.2 Dust and climate change in the tropics

Over the tropics, the simulated negative radiative forcing of the LGM climate by dust is much larger than in the high latitudes, due to the high absolute concentrations of dust and the more extensive ocean areas underneath. The forcing is comparable in magnitude to the negative forcing due to lowered atmospheric CO_2. Our simulated numerical values have considerable uncertainty, in part because available dust deposition data do not allow us to evaluate simulated large dust loading and radiative forcing over e.g. SE Asia and the eastern equatorial Pacific. If the large dust increases we predict over these areas were not upheld by observations then the estimated magnitude of the tropical dust effect would have to be lowered. Nevertheless, our simulation results indicate that the potential contribution of dust to radiative forcing over the tropics is too large to be ignored. This conclusion holds independently of the assumptions made in the different model experiments concerning the mineral mixing state, the strength of the Australian dust source, and the effect of vegetation changes on surface albedo. Recently compiled LGM marine and terrestrial records are converging on an estimated tropical sea-level cooling $\approx$ –3 K (Sonzogni et al. 1998; Farrera et al. 1999). A significant proportion of this cooling may be attributable to dust.

Negative radiative forcing by dust does not translate directly into cooling of the surface climate. The potential surface cooling due to radiative forcing by the additional LGM dust can be roughly bracketed, by applying modelled tropical climate sensitivities (surface temperature change per unit radiative forcing, in K $W^{-1} m^2$). Using the full range of tropical climate sensitivities estimated from LGM simulations performed for the Palaeoclimate Modelling Intercomparison Project (PMIP) (Pinot et al. 1999), together with the uncertainty range in the forcing from experiments 1–3, we estimate that the dust-induced LGM cooling relative to present over the 30°S to 30°N band lies within the bounds –0.8 to –7 K. These actual values are intrinsically unlikely, and the large value of –7 K especially would be hard to reconcile with observations (Sonzogni et al. 1998; Farrera et al. 1999). However, this calculation emphasizes the inherent uncertainty in translating radiative forcing into surface cooling. The release of absorbed energy in the troposphere may also have contributed to reducing convection (Miller and Tegen 1998; Mohalfi et al. 1998) and

precipitation (Hansen et al. 1997) in the tropics. Current understanding of the impact of aerosols on tropical climates likely does not permit a precise quantification of these effects. Progress should be possible nevertheless, by including dust as an active tracer in atmospheric general circulation models, thus closing the feedback loop linking the physical climate to vegetation and dust deflation. We present results here in terms of radiative forcing alone, recognizing that future work must include attempts to simulate the full set of climatic consequences and feedbacks.

4.3 Possible feedbacks among dust, sea-surface temperatures and atmospheric [CO_2]

Cold ocean surface conditions and low atmospheric CO_2 are mutually reinforcing, because of the radiative forcing effect of CO_2 and the effect of temperature on the solubility of CO_2 in surface seawater. Both factors separately contribute to the conditions favouring extensive dust sources (Mahowald et al. 1999). A cold ocean surface generates less precipitation on land, while CO_2 at LGM levels reduces the ratio of plant carbon fixed to water transpired, lowering the sustainable vegetation density in water-limited ecosystems (Farrera et al. 1999; Mahowald et al. 1999). Extensive dust sources in turn may help to maintain low sea surface temperatures in the tropics by radiative mechanisms as shown here, and may be instrumental in maintaining low CO_2 by providing Fe to fertilize marine ecosystems and promote export production in the Southern OceanOcean (Martin 1990; Lefévre and Watson 1999; Watson et al. 2000). Our results therefore support the notion that ice sheets, sea-surface temperatures, dust and CO_2 may be linked through multiple positive feedbacks. In order to further quantify and evaluate this idea, it will be necessary to include atmospheric dust as a fully interactive component of Earth system models with biogeochemical as well as physical components.

References

Andersen KK, Armengaud A, Genthon C (1998) Atmospheric dust under glacial and interglacial conditions. Geophys Res Lett 25: 2281–2284

Barkstorm BR, Harrison EF, Lee RB (1990) Earth radiation budget Experiment, preliminary seasonal results. EOS Transactions, American Geophysical Union 71 (February 27)

Basile I, Grousset FE, Revel M, Petit JR, Biscaye PE, Barkov NI (1997) Patagonian origin of glacial dust deposited in East

Antarctica (Vostok and Dome C) during glacial stages 2, 4 and 6. Earth Planet Sci Lett 146: 573–589

Berger A, Loutre MF (1991) Insolation values for the climate of the last 10 million years. Quat Sci Rev 10: 297–317

Biscaye PE, Grousset FE, Revel M, VanderGaast S, Zielinski GA, Vaars A, Kukla G (1997) Asian provenance of glacial dust (stage 2) in the Greenland Ice Sheet Project 2 Ice Core, Summit, Greenland. J Geophys Res-Oceans 102: 26,765–26,781

Catubig NR, Archer DE, Francois R, deMenocal P, Howard W, Yu EF (1998) Global deep-sea burial rate of calcium carbonate during the last glacial maximum. Paleoceanography 13: 298–310

Claquin T (1999) Modeling of the mineralogy and the radiative forcing of desert dust. PhD Thesis, Paris University, Paris, France

Claquin T, Schulz M, Balkanski Y, Boucher O (1998) Uncertainties in assessing radiative forcing by mineral dust. Tellus Ser B – Chem Phys Meteorol 50: 491–505

Claquin T, Schulz M, Balkanski YJ (1999) Modeling the mineralogy of atmospheric dust sources. J Geophys Res-Atmos 104(D18): 22,243–22,256

CLIMAP Project Members (1981) Seasonal reconstructions of the Earth's surface at the Last Glacial Maximum. Geological Society of America Map Chart Series 36

Cowling SA (1999) Simulated effects of low atmospheric CO_2 on structure and composition of North American vegetation at the Last Glacial Maximum. Global Ecol Biogeogr 8(2): 81–93

Crosta X, Pichon JJ, Burckle LH (1998a) Reappraisal of Antarctic seasonal sea-ice at the Last Glacial Maximum. Geophys Res Lett 25: 2703–2706

Crosta X, Pichon JJ, Burckle LH (1998b) Application of modern analog technique to marine Antarctic diatoms: reconstruction of maximum sea-ice extent at the Last Glacial Maximum. Paleoceanography 13: 284–297

DeAngelis M, Steffensen JP, Legrand MR, Clausen HB, Hammer CU (1997) Primary aerosol (sea salt and soil dust) deposited in Greenland ice during the last climatic cycle: comparison with east Antarctic records. J Geophys Res-Oceans 102: 26,681–26,698

Douville H, Royer JF, Mahfouf JF (1995a) A new snow parametrization for the meteo-France climate model. 1. Validation in stand-alone experiments. Clim Dyn 12: 21–35

Douville H, Royer JF, Mahfouf JF (1995b) A new snow parametrization for the meteo-France climate model. 2. Validation in a 3-D GCM experiment. Clim Dyn 12: 37–52

Farrera I, Harrison SP, Prentice IC, Ramstein G, Guiot J, Bartlein PJ, Bonnefille R, Bush M, Cramer W, von Grafenstein U, Holmgren K, Hooghiemstra H, Hope G, Jolly D, Lauritzen S-E, Ono Y, Pinot S, Stute M, Yu G (1999). Tropical climates at the Last Glacial Maximum: A new synthesis of terrestrial data. I. Vegetation, lake-levels and geochemistry. Clim Dyn 15: 823–856

Foster DJ, Davy RD (1988) Global snow depth climatology. USA/FETAC/TN – 88/006, Scot Air Force Base, Illinois, pp 48

Fouquart Y, Bonnel B (1980) Computation of solar heating of the Earth's atmosphere: a new parametrization. Beitr Phys Atmos 53: 35–62

Hansen JE, Sat M, Ruedy R (1997) Radiative forcing and climate response. J Geophys Res-Atmosphere 102: 6831–6864

Harvey LDD (1988) Climatic impact of ice-age aerosols. Nature 334: 333–335

Haxeltine A, Prentice IC (1996) BIOME3: an equilibrium terrestrial biosphere model based on ecophysiological constraints, resource availability, and competition among plant functional types. Global Biogeochem Cy 10: 693–709

Heimann M (1995) The global atmospheric tracer model TM2, Tech Rep 10, Klimarechenzent, Hamburg, Germany

Hermann JR, Bhartia PK, Torres O, Hsu C, Seftor C, Celarier E (1997) Global distribution of UV-absorbing aerosols from Nimbus 7/TOMS data. J Geophys Res-Atmosphere 102: 16,911–16,922

Hesse PP (1994) The record of continental dust from Australia in Tasman Sea sediments. Quat Sci Rev 13: 257–272

Hewitt CD, Mitchell JFB (1997) Radiative forcing and response of a GCM to ice age boundary conditions: cloud feedback and climate sensitivity. Clim Dyn 13: 821–834

Husar RB, Prospero JM, Stowe LL (1997) Characterization of tropospheric aerosols over the oceans with the NOAA advanced very high resolution radiometer optical thickness operational product. J Geophys Res-Atmos 102: 16,889–16,909

Kaufmann YJ, Tanré D, Dubovik O, Karnieli A, Remer LA (2001) Absorption of sunlight by dust as inferred from satellite and ground-based remote sensing. Geophys Res Lett 28: 1479–1482

Kohfeld K, Harrison S (2000) How well can we simulate past climates? Evaluating the models using global palaeoenvironmental datasets. Quat Sci Rev 19: 321–346

Kohfeld KE, Harrison SP (2001) DIRTMAP: the geological record of dust. Earth Sci Rev 54: 81–114

Kolla V, Biscaye PE (1977) Distribution and origin of quartz in sediments of Indian Ocean. J Sediment Petrol 47: 642–649

Kolla V, Biscaye PE, Hanley AF (1979) Distribution of quartz in Late Quaternary Atlantic sediments in relation to climate. Quat Res 11: 261–277

Leemans R, Cramer W (1991) The IIASA database for mean monthly values of temperature, precipitation and cloudiness of a global terrestrial grid. International Institute for Applied Systems Analysis (IIASA). RR-91-18. Laxenburg, Austria

Lefévre N, Watson AJ (1999) Modeling the geochemical cycle of iron in the oceans and its impact on atmospheric CO_2 concentrations. Global Biogeochem Cy 13: 727–736

Quijano AL, Sokolik I, Toon OB (2000) Radiative heating rates and direct radiative forcing by mineral dust in cloudy atmospheric conditions. J Geophys Res-Atmosphere 105: 12,207–12,219

Mahowald N, Kohfeld KE, Hansson M, Balkanski Y, Harrison SP, Prentice IC, Schulz M, Rodhe H (1999) Dust sources and deposition during the Last Glacial Maximum and current climate: a comparison of model results with paleodata from ice cores and marine sediments. J Geophys Res 104: 15,895–15,916

Markgraf V (1993) Climatic history of Central and South America since 18,000 yr BP: comparison of pollen records and model simulations. In: Wright HE Jr (ed) Global climates since the Last Glacial Maximum. University of Minnesota Press, Minneapolis, pp 357–385

Martin J (1990) Glacial–interglacial CO_2 change: the iron hypothesis. Paleoceanography 5: 1–13

McTainsh GH, Lynch AW (1996) Quantitative estimates of the effect of climate change on dust storm activity in Australia during the Last Glacial Maximum. Geomorphology 17: 263–271

Miller RL, Tegen I (1998) Climate response to soil dust aerosols. J Clim 11: 3247–3267

Mohalfi S, Bedi HS, Krishnamurti TN, Cocke SD (1998) Impact of shortwave radiative effects of dust aerosols on the summer season heat low over Saudi Arabia. Mon Weather Rev 126: 3153–3168

Moller P, Bolshiyanov DY, Bergsten H (1999) Weichselian geology and palaeoenvironmental history of the central Taymyr Peninsula, Siberia, indicating no glaciation during the last global glacial maximum. Boreas 28: 92–114

Monteith JL (1995) Accommodation between transpiring vegetation and the convective boundary layer. J Hydrol 166: 251–263

Morcrette JJ, Fouquart Y (1985) On systematic errors in parametrized calculations of longwave radiation transfer. Q J R Meteorol Soc 111: 691–708

Morcrette JJ, Smith L, Fouquart Y (1986) Pressure and temperature dependence of the absorption of longwave radiation parametrizations. Contrib Phys Atmos 59: 455–469

Overpeck J, Rind D, Lacis A, Healy R (1996) Possible role of dust-induced regional warming in abrupt climate change during the last glacial period. Nature 384: 447–449

Patterson EM (1981) Optical properties of the crustal aerosol: relation to chemical and physical characteristics. J Geophys Res-Ocean-Atmosphere 86: 3236–3246

Peltier WR (1994) Ice Age paleotopography. Science 265: 195–201

Petit JR, Jouzel J, Raynaud D, Barkov NI, Barnola JM, Basile I, Bender M, Chappellaz J, Davis M, Delaygue G, Delmotte M, Kotlyakov VM, Legrand M, Lipenkov VY, Lorius C, Pepin L, Ritz C, Saltzman E, Stievenard M (1999) Climate and atmospheric history of the past 420,000 years from the Vostok ice core, Antarctica. Nature 399: 429–436

Pinot S, Ramstein G, Harrison SP, Prentice IC, Guiot J, Stute M, Joussaume S (1999) Tropical paleoclimates at the Last Glacial Maximum: comparison of Paleoclimate Modeling Intercomparison Project (PMIP) simulations and paleodata. Clim Dyn 15: 857–874

Prentice IC, Jolly D, BIOME 6000 Participant (2000) Mid-Holocene and glacial-maximum vegetation geography of the northern continents and Africa. J Biogeogr 27: 507–519

Rea DK (1994) The paleoclimatic record provided by eolian deposition in the deep sea: the geologic history of wind. Rev Geophys 32: 159–195

Rea DK, Leinen M (1988) Asian aridity and the zonal westerlies: late Pleistocene and Holocene record of eolian deposition in the Northwest Pacific Ocean. Palaeogeogr Palaeoclimatol Palaeoecol 66: 1–8

Roelandt C (2002) Coupled simulation of potential natural vegetation, terrestrial carbon balance and physical land-surface properties with the ALBIOC model. Ecol Modell (in press)

Ruddiman WF (1997) Tropical Atlantic terrigenous fluxes since 25,000 years BP. Marine Geology 136: 189–207

Russell GL, Lerner JA (1981) A new finite–differencing scheme for the tracer transport equation. J Appl Meteorol 20: 1483–1498

Sarnthein M, Tetzlaff G, Koopmann B, Wolter K, Pflaumann U (1981) Glacial and interglacial wind regimes over the eastern subtropical Atlantic and North-West Africa. Nature 293: 193–196

Schulz M, Balkanski Y, Guelle W, Dulac F (1998) Role of aerosol size distribution and source location in a three-dimension simulation of a Saharan dust episode tested against satellite-derived optical thickness. J Geophys Res-Atmosphere 103: 10,579–10,592

Sokolik IN, Toon OB (1996) Direct radiative forcing by anthropogenic airborne mineral aerosols. Nature 381: 681–683

Sokolik IN, Toon OB (1999) Incorporation of the mineralogical composition into models of the radiative properties of mineral aerosol from UV to IR wavelengths. J Geophys Res 104 (D8): 9423–9444

Sonzogni C, Bard E, Rostek F (1998) Tropical sea-surface temperatures during the last glacial period: a view based on alkenones in Indian Ocean sediments. Quat Sci Rev 17: 1185–1201

Steffensen JP (1997) The size distribution of microparticles from selected segments of the Greenland Ice Core Project ice core representing different climatic periods. J Geophys Res-Oceans 102: 26,755–26,763

Tegen I, Fung I (1994) Modeling of mineral dust in the atmosphere: sources, transport, and optical thickness. J Geophys Res-Atmosphere 99: 22,897–22,914

Tegen I, Lacis AA (1996) Modeling of particle size distribution and its influence on the radiative properties of mineral dust aerosol. J Geophys Res-Atmosphere 101: 19,237–19,244

Thompson LG, Mosley-Thompson E (1981) Microparticle concentration variations linked with climatic change: evidence from polar ice cores. Science 212: 812–815

Volz FE (1973) Infrared optical constants of ammonium sulfate, Sahara dust, volcanic pumice, and flyash. App Opt 12: 564–568

Watson AJ, Bakker DCE, Ridgwell AJ, Boyd PW, Law CS (2000) Effect of iron supply on Southern Ocean CO_2 uptake and implications for glacial atmospheric CO_2 Nature 407: 730–733

Weinelt M, Sarnthein M, Pflaumann U, Schulz H, Jung S, Erlenkeuser H (1996) Ice-free nordic seas during the last glacial maximum? Potential sites of deepwater formation. Paleoclimates 1: 283–309

Yung YL, Lee T, Wand CH, Shieh YT (1996) Dust: a diagnostic of the hydrologic cycle during the Last Glacial Maximum. Science 271: 962–963